Examination of an Interior Permanent Magnet Type Axial Gap Motor for the Hybrid Electric Vehicle

Tatsuro Arakawa[1], Masatsugu Takemoto[1], Satoshi Ogasawara[1],
Koji Inoue[2], Osamu Ozaki[2], Hirofumi Hojo[2], and Hiroyuki Mitani[2]

[1] Graduate School of Information Science and Technology, Hokkaido University, Sapporo, Hokkaido, Japan
[2] Kobe Steel, Ltd., Kobe, Hyogo, Japan

Abstract -- Hybrid electric vehicles (HEVs) that emit less carbon dioxide have attracted much attention and rapidly become widespread, but further popularization of HEVs requires further technical advancement of mounted traction motors. Accordingly, our research group focuses on axial gap motors that can realize high torque density. In this paper, an axial gap motor with a novel interior permanent magnet (IPM) rotor structure is proposed and an examination of the proposed motor at the actual motor size of an HEV is presented. For comparison, we selected the newest radial gap-type 60 kW IPM synchronous motor equipped in the third-generation Toyota Prius. Under the condition that the size of the proposed motor be the same as the comparison motor, we confirmed through three-dimensional finite-element analysis that the proposed motor could output twice the maximum torque of the comparison motor. In addition, a comparison was made with a previously reported conventional IPM-type axial gap motor, and the proposed motor was found to be more effective in generating reluctance torque. Moreover, the proposed motor exhibited sufficient durability to irreversible demagnetization of the permanent magnets, to stress caused by rotating the rotor, and to unbalanced electromagnetic forces caused by axial rotor eccentricity.

***Index Terms*—Permanent magnet synchronous motor, Hybrid electric vehicle, Axial gap motor, Interior permanent magnet rotor structure**

I. Introduction

Recently, public concern about environmental issues such as global climate change has grown and various technologies have been considered. Within this context, improving the energy use efficiency of automobiles is required in order to limit emissions of carbon dioxide gas. Hybrid electric vehicle (HEV) technologies, which contribute to reducing global warming, have thus attracted increased attention, and HEV market penetration has been increasing rapidly. For further advancement of HEV dissemination, electric traction motors with sophisticated performance, such as small size, high power density, and high efficiency, are necessary.

References [1]-[4] examined axial gap motors with feasibility for high torque density performance. Our research group therefore focuses on axial gap motors. However, it is difficult for general axial gap motors, such as surface permanent magnet (SPM)-type or inset-type motors, to realize a wide speed range of constant output [5], a requirement for HEV driving systems. The IPM-type axial gap motor was therefore proposed as an axial flux interior permanent magnet (AFIPM) motor in [6] and [7]. This motor can realize a wide speed range of constant output, but it is difficult for this motor to generate reluctance torque effectively. Additionally, no previous studies have attempted to apply this motor to the actual motor size of an HEV motor, for example, a 60 kW motor.

Accordingly, this paper proposes a novel IPM-type axial gap motor equipped with leakage poles that pierce the rotor in the axial direction. In the proposed motor, the leakage poles can effectively generate reluctance torque. This paper examines the proposed motor applied to a 60 kW electric traction motor. In addition, analysis results of three-dimensional finite-element analysis (3D-FEA) are discussed in detail.

II. Structure of the Proposed IPM-Type Axial Gap Motor

Table I shows comparison and target values for the proposed motor. Comparison values are based on the newest radial gap-type 60 kW motor mounted in the third-generation Toyota Prius, a commercialized HEV [8]. The size of the comparison motor was measured in our laboratory. The target values of the proposed motor were set with a goal of 400 Nm output, about twice the torque of the same-sized comparison motor. The maximum output power of the proposed motor was the same as that of the 60 kW motor. With an increase in torque, the torque density increased and the rated speed decreased. In this study, the maximum current density was set

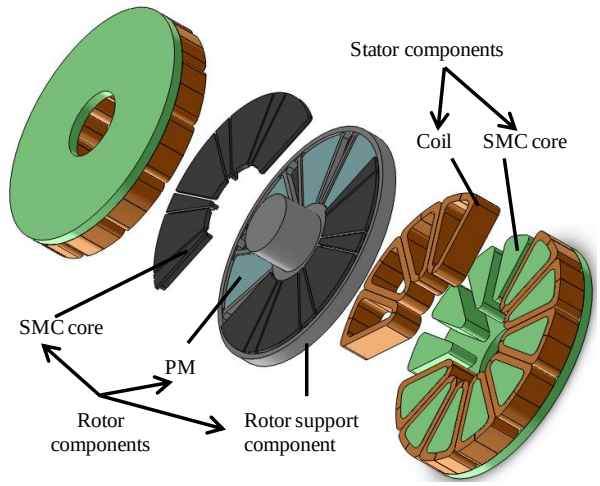

Fig. 1. Outline of the proposed IPM type axial gap motor.

TABLE I
TARGET VALUES OF THE PROPOSED MOTOR

	Comparison value	Target value
Max. torque	207 Nm	400 Nm
Volume	5.91 L	5.91 L
Max. torque density	35.0 Nm/L	67.7 Nm/L
Max. power	60 kW	60 kW
Rated speed	2768 rpm	1464 rpm
Max. speed	13900 rpm	6000 rpm
Max. current density	20 Arms/mm^2	20 Arms/mm^2

TABLE II
SPECIFICATIONS OF THE PROPOSED MOTOR

Outer diameter of motor	264 mm
Total motor axial length	108 mm
Rotor thickness	26 mm
PM thickness	10 mm
Arc angle of PM	34°
Number of poles	8
Number of slots	12
Slot fill factor of coil	57.3%
Air gap	1.5 mm

to 20 Arms/mm^2.

Fig. 1 shows the outline of the proposed motor. This motor is an axial gap type, and thus both the rotor and stators are on the same rotation axis. Furthermore, the motor is an internal-rotor-external-stator type in which a single rotor is sandwiched by two stators.

As for the rotor structure, high-performance neodymium permanent magnets are sandwiched by two soft magnetic component (SMC) cores. The permanent magnets are arranged between rotor support components made of nonmagnetic steel, as shown in Fig. 2. This structure forms the IPM structure. Fig. 2(a) shows the conventional rotor structure in [6] and [7]. In the conventional rotor structure, thin SMC cores are located on the surface of the rotor support component. These thin SMC cores are called leakage poles. Fig. 2(b) shows the novel rotor structure proposed in this paper. The leakage poles with SMC cores pierce the rotor support component in the axial direction. By arranging the leakage poles between the permanent magnets, *q*-axis flux can easily pass through the leakage poles in the axial direction. Because the inductance L_q of the *q*-axis in the proposed motor is higher than that in the conventional motor, the proposed motor can make effective use of reluctance torque.

The stator cores are composed of SMC material. The three-phase concentrated stator winding is wound around 12 stator teeth. In the proposed motor, the gap length of one side between the rotor and the stator is a relatively wide gap of 1.5 mm. Other specifications are indicated in Table II.

III. RESULTS OF 3D-FEA

3D-FEA of the proposed motor was carried out by using JMAG Studio simulation software for the development of electrical devices. This paper presents the results of analysis of torque characteristics and resistance to irreversible demagnetization of the permanent magnets. Moreover, we used SolidWorks 3D CAD software to investigate the durability to stress caused by rotating the rotor.

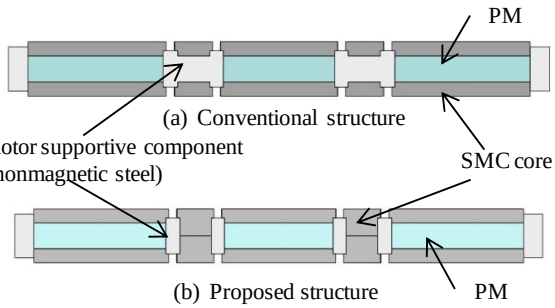

Fig. 2. Cross sections of the conventional and proposed rotor structures in IPM-type axial gap motors.

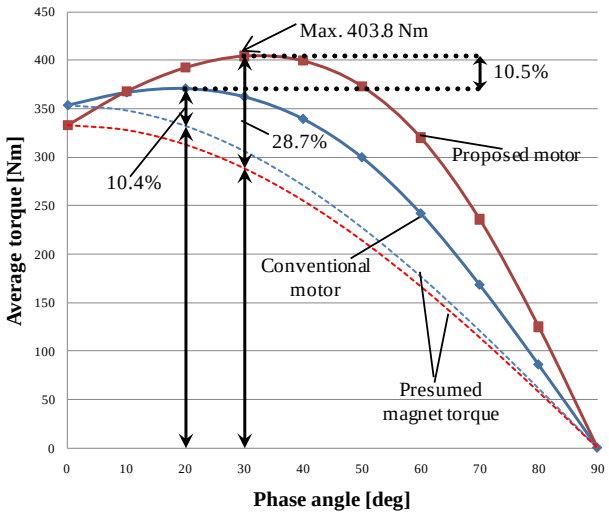

Fig. 3. Relationship between phase angle and average torque. This graph shows the results of analysis of the conventional and proposed motors.

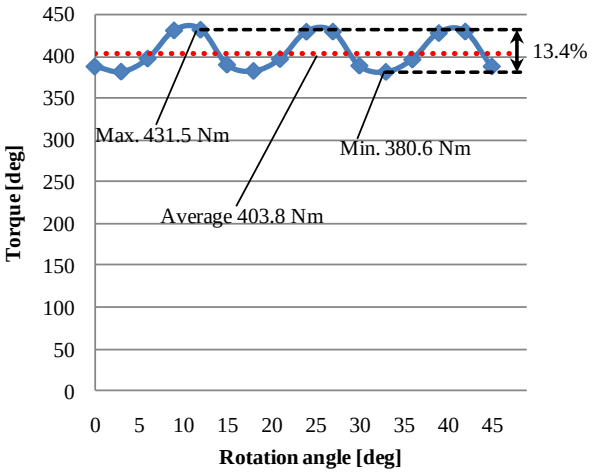

Fig. 4. The relationship between rotation angle and instantaneous torque at a rated current of 20 Arms/mm^2 and a phase angle of 30°. The peak-to-peak torque ripple is 13.4%.

A. Torque Characteristics

Fig. 3 shows the relationship between average torque and phase angle at a rated current of 20 Arms/mm^2. The temperature of the permanent magnets was constant at 75 °C. In the proposed motor, the maximum average torque was 403.8 Nm when the phase angle was 30°, fulfilling the target value shown in Table I. Torque density reached 68.3 Nm/L.

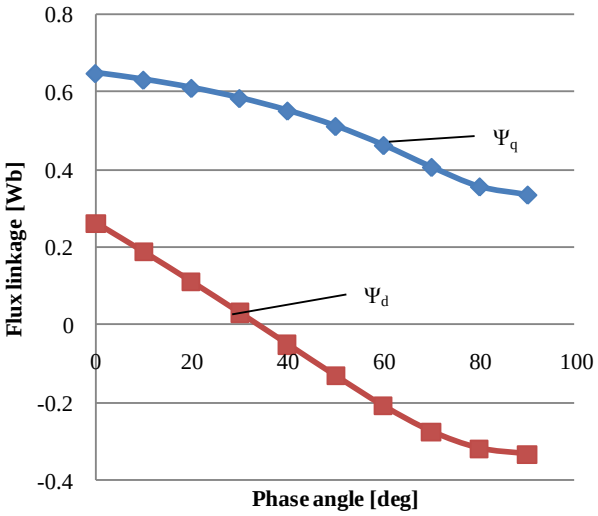

Fig. 5. Relationship between phase angle and the *d*- and *q*-axis flux linkage.

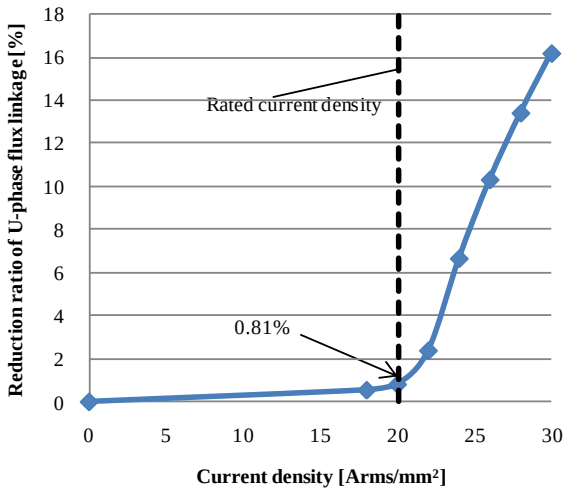

Fig. 6. Relationship between current density and the reduction ratio of U-phase flux linkage.

Compared with the comparison motor that is the newest radial gap motor mounted in commercially-supplied HEVs, the proposed motor could achieve a torque density of more than 1.95 times higher, while retaining the same size. A maximum output power of 60 kW was achieved at 1419 rpm. Compared with the 2768 rpm of the comparison motor, the rated speed could be reduced by 48.7%. The short dashed line shows the magnet torque presumed from the average torque at a phase angle of 0°. When the maximum average torque was generated at a phase angle of 30°, the ratio of the reluctance torque was 28.7% (Fig. 3).

Fig. 3 presents the analysis results for the conventional motor shown in Fig. 2(a) in order to compare it with the proposed motor. The analysis conditions of the two motors are very similar, excluding the shape of the leakage poles (see Fig. 2). In the conventional motor, the maximum average torque was 365.5 Nm when the phase angle was 20°. At that time, the ratio of reluctance torque was 10.4%.

The ratio of the reluctance torque was 28.7% for the proposed motor, which was higher than the 10.4% of the conventional motor. It was found that reluctance torque could be effectively generated in the proposed motor equipped with leakage poles that pierce the rotor in the axial direction. Consequently, the maximum average torque of the proposed motor was 10.5% higher than that of the conventional motor.

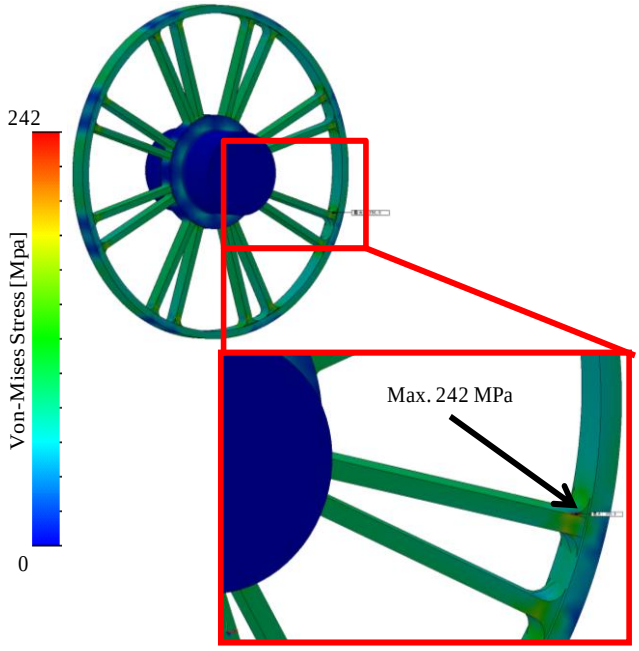

Fig. 7. Three-dimension stress analysis result of the rotor at the maximum rotation speed of 6000 rpm.

Fig. 4 shows the relationship between instantaneous torque and rotational angle when the maximum average torque of the proposed motor was generated at a rated current of 20 Arms/mm^2 and a phase angle of 30°. The peak-to-peak torque ripple of the proposed motor was sufficiently small at 13.4%.

Fig. 5 shows the relationship between the *d*- and *q*-axis flux linkages and phase angles at a rated current of 20 Arms/mm^2. As this figure makes clear, the *d*-axis flux linkage Ψ_d was changed from a positive value to a negative value by increasing the phase angle. Therefore, the proposed motor can be driven with field weakening control. Also, a wide range of constant output can be expected.

B. Durability to Irreversible Demagnetization of Permanent Magnets

Fig. 6 shows the reduction ratio of the U-phase flux linkage generated by the permanent magnets. This is an index that indicates the state of irreversible demagnetization of the permanent magnets caused by employing a very high current density. The reduction ratio δ is defined as follows:

$$\delta = \frac{\Psi_{mb} - \Psi_{ma}}{\Psi_{mb}} \times 100[\%], \qquad (1)$$

where Ψ_{mb} is the U-phase flux linkage generated by the permanent magnets before the current is conducted, and Ψ_{ma} is that after the current is conducted. For each plot of Fig. 6, the 3D-FEA analysis was carried out under the following conditions while changing the current density: the phase angle was constant at 90° because the field weakening flux at the phase angle of 90° was exactly opposite the magnetizing

direction of the permanent magnets, and the temperature of the permanent magnets was held constant at 150 °C to reproduce harsh conditions for the permanent magnets, because irreversible demagnetization progresses easily at high temperatures.

The reduction ratio δ increased rapidly when the conducted current exceeded a rated current of 20 Arms/mm^2. It is known that irreversible demagnetization of permanent magnets progresses more rapidly than at a rated current. In the proposed motor, however, the reduction ratio δ was only 0.81% at the rated current. This result confirms that the proposed motor had good endurance against irreversible demagnetization under a rated current.

C. Durability to Stress Caused by Rotating Rotor

Another important consideration for motors is that rotor stress increases in proportion to the square of the rotational speed. Therefore, stress analysis was also executed. The maximum rotational speed of the proposed motor is 6000 rpm, and thus the analysis was carried out at 6000 rpm.

Fig. 7 shows the analysis results. The maximum stress was 242 MPa at the location indicated by the arrow. The 18Mn-18Cr austenitic steel used for the rotor support component has at least 450 MPa yield strength. Accordingly, the analysis was executed under the condition that the yield strength was 450 MPa. The safety factor in the rotational speed was therefore a sufficiently high value of 1.36.

D. Durability to Unbalanced Electromagnetic Force Caused by Rotor Eccentricity

Rotor eccentricity in the axis direction causes unbalanced electromagnetic forces acting on the rotor in the same direction. This is one factor that can cause overloading of the motor bearings, causing extensive bearing loss. Accordingly, we carried out an analysis of rotor eccentricity.

Fig. 8 shows the relationship between unbalanced electromagnetic force and rotor eccentricity. The analysis was executed under conditions of a current density of 20 Arms/mm^2 of the rated current and a phase angle of 30°. The rotor eccentricity was increased from 0 mm to 0.1 mm in 0.025 mm steps. The unbalanced electromagnetic force was proportional to the rotor eccentricity, and the force was 448.4 N when the rotor eccentricity was 0.1 mm. An angular contact-type ball bearing with 4500 N permissible load in the axial direction is planned to be used in the proposed motor. Therefore, the unbalanced electromagnetic force of the proposed motor was less than 10% of the permissible load.

IV. Conclusion

This paper proposed an axial gap motor with a novel IPM-type rotor structure. The proposed motor has leakage poles that pierce the rotor in the axial direction. Since *q*-axis flux can easily pass through the leakage poles in the axial direction, the proposed motor can make effective use of reluctance torque.

As a target for comparison, we selected the newest radial gap-type 60 kW motor mounted in the Toyota Prius, a commercialized HEV. The target values of the proposed motor were set with a goal of outputting 400 Nm, about twice the torque of the same-sized comparison motor.

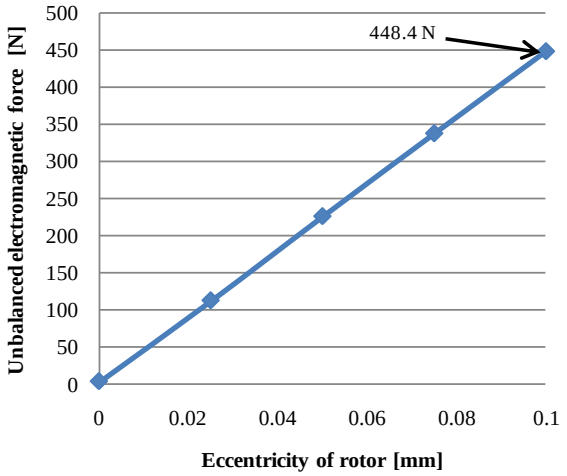

Fig. 8. Relationship between unbalanced electromagnetic force and rotor eccentricity.

Analysis results indicated that the proposed motor had a maximum average torque of 403.8 Nm. Compared with the comparison motor, the proposed motor could achieve a torque density of more than 1.95 times higher while retaining the same size. Moreover, we confirmed that the proposed motor had sufficient durability against irreversible demagnetization of the permanent magnets and the stress caused by rotating the rotor. We conclude that the proposed motor has sufficient performance for practical use.

References

[1] M. Aydin, S. Huang, and T. A. Lipo "Torque Quality and Comparison of Internal and External Rotor Axial Flux Surface-Magnet Disc Machines", *IEEE Trans. Ind. Electronics*, Vol. 53, No. 3, pp. 822-830, June 2006.

[2] M. Aydin, S. Huang, and T.A. Lipo, "Axial Flux Permanent Magnet DiscMachines: A Review", in *Conf. Record of SPEEDAM*, pp. 61-71, May 2004.

[3] T. J. Woolmer and M. D. McCulloch, "Analysis of the Yokeless And Segmented Armature Machine", in *Proc. 2007 IEEE Int. Electric Machines and Drives Conf.* (IEMDC '07), pp.704-708, 2007.

[4] W. Fei, P. Luk, and K. Jinupun, "A new axial flux permanent magnet Segmented-Armature-Torus machine for in-wheel direct drive applications", in *Proc. 2008 IEEE* Power Electronics Specialists Conf. (PESC 2008), pp.2197-2202, 2008.

[5] K. M. Rahman, N. R. Patel, T. G. Ward, J. M. Nagashima, F. Caricchi, and F. Crescimbini, "Application of Direct-Drive Wheel Motor for Fuel Cell Electric and Hybrid Electric Vehicle Propulsion System" *IEEE Trans. Ind. Applicat.*, Vol. 42, No. 5, pp.1185-1192, Sep./Oct. 2006.

[6] A. Cavagnino, M. Lazzari, F. Profumo, and A. Tenconi "Axial Flux Interior PM Synchronous Motor: Parameters Identification and Steady-State Performance Measurements" *IEEE Trans. Ind. Applicat.*, Vol. 36, No. 6, pp. 1581-1588, Nov./Dec. 2000.

[7] F. Profumo, A. Tenconi, Z. Zhang, and A. Cavagnino, "Novel Axial Flux Interior PM Synchronous Motor Realized with Powdered Soft Magnetic Materials", in *Conf. Rec. IEEE-IAS 1998 Annu. Meeting*, Vol. 1, pp.152-158, Oct. 1998.

[8] TOYOTA MOTOR CORPORATION, Web Page of PRIUS Specs, "http://www.toyota.com/prius-hybrid/specs.html"